Nano–porous Network of DMTD–Ag Coordination Polymer for the Ultra Trace Detection of Anticholinergic Drug

3.1 Introduction

Nano–porous coordination polymers (NPCPs) constructed from metal ions and organic bridging ligands have emerged as magnificent materials because of their high structural regularity and diversity, easy modification of frameworks, lack of non–accessible bulk volume, high porosity and structural flexibility [Yaghi et al., 2003; Kitagawa et al., 2004; Bradshaw et al., 2005; Férey et al., 2008; Valtchev et al., 2013; Foo et al., 2014; Meek et al., 2011]. They have been frequently used in various applications such as gas storage, gas separation, optical sensing, shape/size selective catalysis, drug delivery, imaging and sensing [Makal et al., 2012; Liu et al., 2015; Hwang et al., 2013; Ranft et al., 2015; Dhakshinamoorthy et al., 2013]. For better practical industrial and biological applications, however, we must consider costs, and safety of NPCPs in addition to their porous performances. In particular nano–porous coordination polymer networks that exhibit conductive properties have enormous potential applications in the fabrication of luminescent materials, fuel cells and sensors [Orcajada et al., 2010]. Moreover, the NPCPs have exclusively used as non–toxic drug delivery shuttles for the delivery of challenging anti–tumoral and retroviral drugs against cancer and AIDS [Keskin et al., 2011]. To the best of our knowledge, there exists no report for the use of NPCPs in drug sensing applications. The design and synthesis of NPCPs using easily available designated ligands and metal components is the focal point of current research [Yoon et al., 2013]. The careful screening and selection of appropriate ligands is quite important because the minor structural changes at the ligand backbone can potentially alter the architecture of the ensuing NPCPs. Silver (I) is an attractive metal having striking coordination numbers ranging from 2 to

8 and with varied coordination geometries [Lee et al., 2010]. The overall structural arrangement of the participating components in the silver(I)–based NPCPs (Ag–NPCPs) are influenced by the ligand design, counter anion, metal to ligand ratio and a few other parameters. These Ag–NPCPs exhibit extensive properties like photoluminescence, photochromism, catalysis, conduction and chiral sensing [Zhang et al., 2013; Konaka et al., 2003; Geng et al., 2012; Zheng et al., 2013; Zhang et al., 2015]. The Ag (I) acts as a soft acid and favors coordination to soft bases such as S and unsaturated N–containing ligands which act as linker in coordination polymers. The soft ligands containing thiadiazole group, i.e. 2,5–dimercapto–1,3,4–thiadiazole (DMTD) is of great interest owing to its latent assembly for building NPCPs with fascinating topologies and properties. This is due to the presence of four chelating sites (two diazole nitrogen and two sulfydryl sulfur donors) that are feasible for coordination particularly with metallic soft acids. Silver(I) NPCPs with 2,5–dimercapto–1,3,4–thiadiazole (DMTD) giving rise to a fascinating array of geometric configurations and architectures similar to Au (I) clusters [Tiwari et al., 2014].

Drug molecule sensing and analysis is the most crucial step not only in drug quality control but also in clinical analysis due to its significant impact on human health and security. Several life saving drugs and fastest growing class of synthetic illicit drugs may become fatal if the doses are exceeding a certain limit [Biavardi et al., 2014]. A variety of analytical methods have been developed to detect drug molecule including solid–phase extraction followed by gas chromatography/mass spectrometry (GC–MS) or liquid chromatography/mass spectrometry (LC/MS), ion trap mobility spectrometry, GC–FT–IR and immunoassay methods. However, these methods are expensive, generally suffer from long operation time and require sophisticated experimental

procedures. Therefore, the development of sensitive, selective and simple methods for the drug analysis are valuable and necessary. The sensitivity and activeness of the matrix of a sensor decides its rapid on–site sophistication for the detection of a drug molecule. So, we envisioned that the unconditional tunability of Silver(I) NPCPs and their ability to interact with various functional groups through entrapment of molecules or ions constitute an advantage over other conventional sensory materials in signal–transduction strategy of sensing [Evans et al., 2014; Liang et al., 2014; Tan et al., 2013]. Atropine sulfate is an alkaloid which is the monohydrate of (1R,3R,5S)–3–tropoyloxytropanium sulfate. It is anticholinergic agent in premedication of anesthesia and can be employed to suppress unstriated muscle controlling glandular secretion [Catch et al., 1960; Maffii et al., 1960]. Its doses greater than 71.90 μM can be fatal while the minimum lethal dose is 107.90 μM. Therefore, the efficacy and toxicity of atropine sulfate should be re–evaluated. To ensure treatment efficacy, it is essential to manage the quality of pharmaceutical products through precise detection of atropine sulfate in the raw material and finished formulations [Baselt et al., 1995; Nash et al., 1953].

To date, several analytical techniques like the atomic absorption method (AAS) [Elries et al., 2001], high–performance liquid chromatography (HPLC) [Pohjola et al., 1994, gas chromatography (GC) [Gupta et al., 1999], thin–layer chromatography (TLC) [Greenwood et al., 2002], chemilluminescence (CL) [Song et al., 2001], spectrophotometry and electro–analytical technique [Lei et al., 2013] have been explored for assay of atropine sulfate. However, the preliminary sample cleaning procedure by chromatographic technique is tedious and time–consuming while utility of spectrophotometry is limited to low sensitivity particularly in low concentration. The

electro–analytical techniques are shown to be excellent for detection of pharmaceutical molecules in various matrices. Many of the active constituents of formulations, in contrast to excipients, can be readily oxidized [Genereux et al., 2010; Mashat et al., 2012; Gassensmith et al., 2014]. Voltammetry is efficiently used in the field of organic and inorganic chemistry, environmental and biochemistry. The effectiveness of voltammetry is consequences of its capability for quickly observing the redox behavior over a vast potential range, but its quantitative employment is restricted due to the inconveniently shaped asymmetric i–E curves detected in the presence of significant charging current at faster scan rates. That's why in this report differential pulse voltammetry (DPV) is used in order to remove these issues [Murugappan et al., 2014; Muniz et al., 2012; Wang et al., 2014; Christie et al., 1965]. Recently atropine is detected over modified electrodes using additives like ion selective molecules (e.g. β–Cyclodextrin) or mediators (e.g. europium(III)–doped Prussian blue), but they are limited due to their detection limit and sensitivity. NPCPs is a better choice for electrode modification due to its multi–catalytic sites and easy diffusion of ions through veins [Li et al., 2005; Zhou et al., 2011; Hou et al., 2008; Xie et al., 2010]. We report a facile one pot synthesis of DMTD–Ag without any chain initiator and characterized by FT–IR, Raman, UV–Vis, XRD, XPS, SEM, TEM and TGA/DTA for its structural, morphological and thermal features. After that DMTD–Ag is used as conducting matrix for the modification of carbon paste electrode (DMTD–Ag/CPE) in the ultra–trace level electrochemical assay of atropine sulphate.

3.2 Experimental

3.2.1 Materials

2,5–Dimercapto–1,3,4–thiadiazole (DMTD) was purchased from Sigma Aldrich. Atropine sulphate, silver nitrate, ethanol, sodium hydroxide, borax from SRL, India were used as received unless otherwise mentioned and atropine sulphate was freshly prepared just before use by consecutive dilution with doubly deionized water. The electrode used for fabrication of carbon paste electrode was obtained from Bioanalytical Systems. The glassware used in the synthesis of polymer was cleaned with freshly prepared aqua regia (3:1, HCl/HNO_3) and comprehensively rinsed with ultrapure water (Merck India). Eye drop (Atropine sulphate I.P. 1% w/v, phenyl mercuric nitrate I.P. 0.001% w/v) were purchased from a local convenience supplier (Jawa Pharmaceuticals, India, Pvt. Ltd.) that diluted with phosphate buffer and pH was adjusted 10 by adding sodium hydroxide and utilized within a day of purchase. All reagents and chemicals used were of analytical grade.

3.2.2 Synthesis of DMTD–Ag

DMTD–Ag material was synthesized simply by the addition of their individual precursors dissolved in ethanol at room temperature. In this synthesis process, 25.0 mM $AgNO_3$ salt was prepared in ethanol and added slowly to the 17.70 mM ethanolic solution of 2,5–dimercapto–1,3,4–thiadiazole under continuous stirring condition. After that resulting reaction mixture was left as such for 20 hrs under thin stream of nitrogen purging. A grey precipitate obtained was purified by washing several times with water and ethanol in order to remove unreacted residue and preserved for further experimentation. The resulting precipitate was tested in various solvents like DMF,

toluene, DMSO, methanol and water for its stability. The yield obtained was 76% after drying.

3.2.3 Instrumentation

Fourier transforms infrared (FT–IR) spectra in KBr pellets were recorded from 2500 to 400 cm^{-1} with FT–IR spectrometer (Nicolet–6700, USA). Raman spectra were measured with a Micro Raman Spectrometer at 180° scattering geometry (Renishaw, Germany) at room temperature with a 514.5 nm line of an Ar+ laser at 50 mW. UV–Vis absorption were executed using Perkin Elmer Lambda–25 spectrophotometer (obtained under DAAD Instrument grant, Germany) by using a quartz cuvette with optical path length of 1 cm. Thermo–gravimetric analysis (TGA) was performed on Mettler Tuldeo (TGA/DSC 1 STARE System, Switzerland) at the rate of 20 °C min^{-1} in nitrogen atmosphere. X–ray diffraction pattern for powder samples of coordination polymer DMTD–Ag was carried out with 18 kW rotating anode powder X–ray diffractometer from 10° to 80°, Rigaku, Japan with Cu–Kα radiation operating in Bragg–Brentano geometry and fitted with a graphite monochromator in diffracted beam with 3°min^{-1} scan rate. Elemental analysis was recorded with X–Ray photoelectron, Kratos Analytical Instrument, Shimadzu group company Amicus XPS, UK. All voltammetric experiments was performed at Ω Metrohm 797 VA Computrace (ion analyzer, Switzerland) through electrochemical software version 3.1 using three electrodes assembly consisting DMTD–Ag modified carbon paste electrode (DMTD–Ag/CPE) as a working electrode, Pt foil as counter electrode and Ag/AgCl as reference electrode for all electrochemical measurements. Phosphate buffer (pH 10.0) was used as a supporting electrolyte and 50 mV/sec scan rate was fixed for each measurement. TEM was performed on TEM Tecnai G2 20 S–Twin Fei, Neitherlands.

3.2.4 Construction of DMTD–Ag/CPE

The CPE was constructed by electrode body with a well of diameter 1 mm purchased from Bioanalytical Systems (West Lafayette, IN; MF 2010). The electrode well was filled with a mixture of an active paste of 67.5% w/w graphite powder, 2.5% w/w DMTD–Ag and 30% w/w nujol oil. After that, the as–filled paste electrode was smoothed on a clean butter paper in order to obtain a flat surface. Similar method is adopted for the unmodified CPE preparation.

3.3 Results and Discussion

DMTD act as soft base for Ag(I) (soft acid) due to the presence of hetro atoms–nitrogen and sulphur, thus resulting into an excellent network in which Ag(I) get coordinated with sulphur atoms of DMTD into the infinite array of polymeric chain. The interaction in as–synthesized DMTD–Ag material is analyzed by FT–IR, Raman, XPS, XRD, UV–Vis and discussed later one by one.

3.3.1 Structural, Morphological and Thermal Analysis

The interaction between DMTD and Ag in DMTD–Ag is analyzed by FT–IR spectra as depicted in figure 3.1. In case of DMTD, there are weak vibrational bands in the region 2450–2350 cm^{-1} resulting from C–H Fermi resonance and stretching overtones. The salient features of spectra include the C–S–C, C=N symmetric and asymmetric stretches appearing at 640 and 1415 cm^{-1} respectively. Note that, a strong band at 1031 cm^{-1} in the spectrum is attributed due to the N–N stretch. Further in DMTD–Ag spectra, the asymmetric stretching frequency of C=N is observed at 1325 cm^{-1} while the vibrational peak at 970 cm^{-1} is assigned for N–N stretching. The contamination of poly(DMTD) is absent in DMTD–Ag as it lacks of the disulfide stretching band near 520 cm^{-1}. Reduction in intensity and diminution in stretching

frequency of C=N in DMTD–Ag indicates an interaction of sulphur atom with Ag, which is also investigated by Raman spectroscopy.

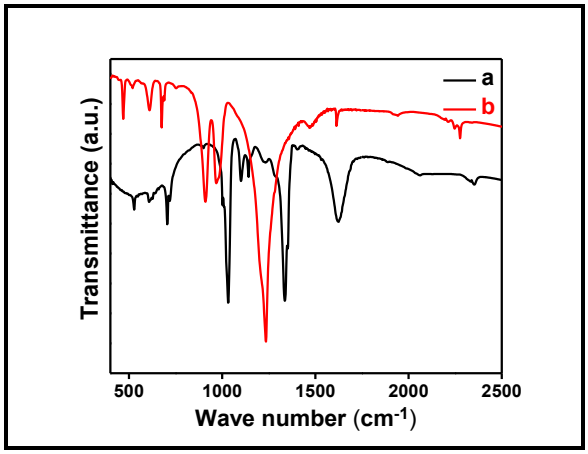

Figure 3.1 FT–IR spectra of (a) DMTD and (b) DMTD–Ag.

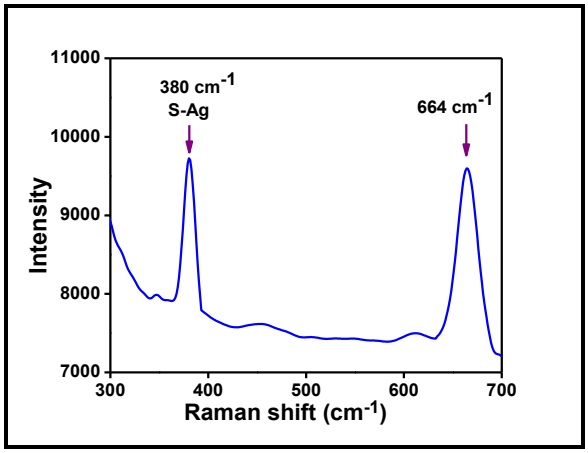

Figure 3.2 Raman spectrum of DMTD–Ag.

The binding interaction behavior in DMTD–Ag is analyzed using Raman spectroscopy (Figure 3.2). The vibrational peak appearing at 380 cm^{-1} is assigned due to S–Ag bond ensuring metal–sulphur linkage [Zaidi et al., 1977] while vibrational frequency at 664 cm^{-1} corresponds to the endocyclic C–S–C symmetric stretch. Thus from the FT–IR and Raman spectrum results it is clear that Ag metal get coordinated by sulphur atoms of DMTD molecules. The variation in UV–Vis absorption spectra of

DMTD–Ag with respect to DMTD is depicted for their interaction (Figure 3.3). DMTD displays two absorption peaks at 354 nm and 270 nm due to n–π* and π–π* transitions respectively [Thorn et al., 1960], while DMTD–Ag exhibit a strong feature centered at 324 nm due to n–π* and 275 nm corresponding to π–π* transition. The hypsochromic shift in the absorption spectra of DMTD–Ag (Inset, Figure 3.3), is due to interaction of DMTD with Ag [Khalil et al., 2012]. Further, the diffraction features of DMTD–Ag and DMTD is analyzed by XRD and compared with Ag(0) obtained from JCPDS file CAS number 89–3722. DMTD–Ag exhibits a high amorphous background along with some sharp peaks resulting due to the presence of small crystallites of low apparent order in polymeric chain [Joshi et al., 2013] (Figure 3.4a). DMTD and Ag(0) exhibit strong diffraction peaks due to their crystalline nature. Owing to these diffraction pattern, it is evident from figure that the structural features of DMTD and Ag(0) are absent in DMTD–Ag. Further the amorphous nature of DMTD–Ag is also investigated by SAED of TEM and discussed later. The oxidation state of Ag in DMTD–Ag is investigated by XPS (Figure 3.5). The best fit for Ag is achieved with two doublets drawn by XPS Peak 4.1 software. The doublets with binding energy at 366.5 eV and 372.6 eV corresponds to the $3d_{5/2}$ and $3d_{3/2}$ of Ag(I) [Fan et al., 2014]. The S(2p) spectrum is fitted into two doublets corresponding to two sulphur atoms present in different chemical environment. The binding energy at 160.5 eV is attributed due to S ($2p_{3/2}$) of aromatic sulphur, and 161.3 eV is due to the sulphur coordinated to the Ag [Bastus et al., 2009; Cui et al., 2011].

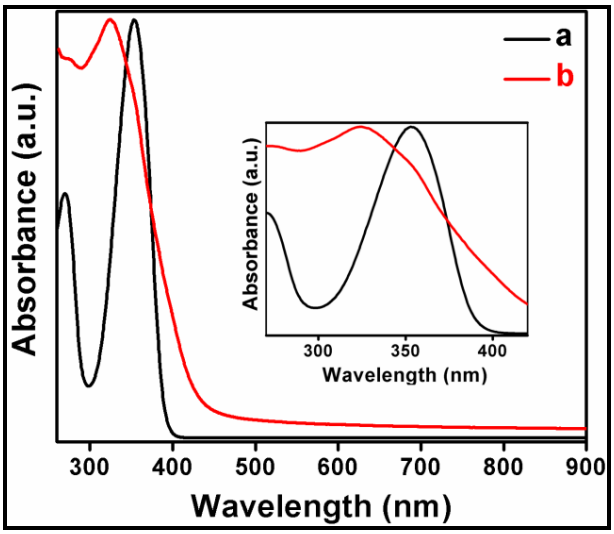

Figure 3.3 UV–Vis absorption spectra of (a) DMTD and (b) DMTD–Ag. Inset shows the enlarge view in range of 270 nm–420 nm.

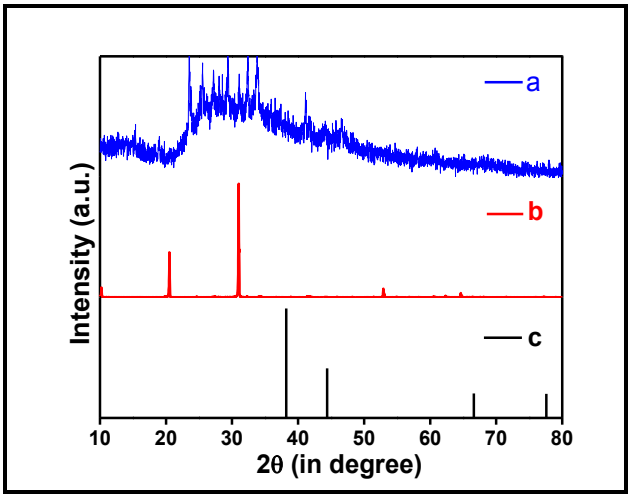

Figure 3.4 XRD of (a) DMTD–Ag (b) DMTD and (c) Ag(0) obtained from JCPDS file CAS number 89–3722.

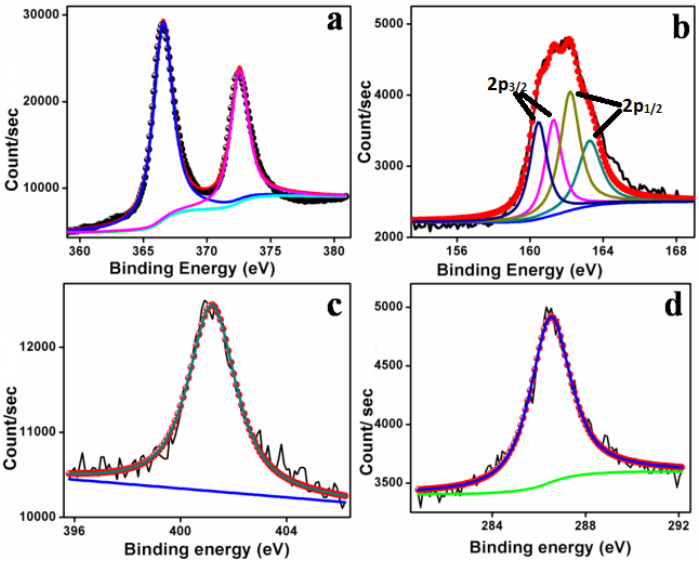

Figure 3.5 XPS spectra of the DMTD–Ag, (a) Ag(3d) (b) S(2p) (c) N(1s) and (d) C(1s) binding energy spectrum.

The binding energy of N(1s) (400.2 eV) is in agreement with results reported for N–N [Xu et al., 2003; Yang et al., 2010]. The C(1s) peak fitted at 286.5 eV is characteristic of C=N bonding. The decrease in the binding energy is caused by the electronegative substituent near the vicinity of carbon atoms. The morphology and elemental analysis of as–synthesized DMTD–Ag is examined by SEM, TEM and EDX (Figure 3.6). It is evident that DMTD–Ag appears as porous and highly packed vein like interconnecting network, resulting from coalesces of nano globular shaped DMTD–Ag (Figure 3.6a and 3.6b). The individual shape of DMTD–Ag is in irregular globules also seen in TEM micrograph (Figure 3.6c). The porous structure is the basis of diffusion controlled electron transfer kinetics as discussed in electrochemical studies. As–synthesized DMTD–Ag is highly amorphous in nature as evident from SAED of TEM image. It is already checked by XRD experimentation discussed above. The chemical composition of the DMTD–Ag is examined by energy dispersive X–ray of SEM

micrograph which reveals the existence of C, N, S and Ag atoms within selected area (Figure 3.6e).

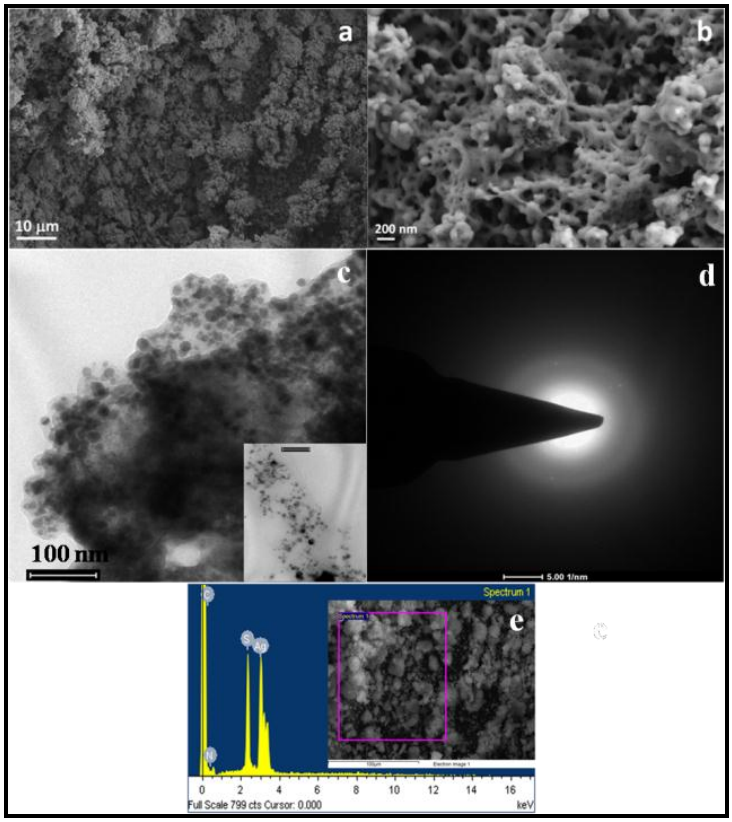

Figure 3.6 (a), (b) FE–SEM, (c) TEM, (d) corresponding SAED pattern and EDX pattern for FE–SEM of DMTD–Ag.

Further, the molecular mechanics calculation is executed in order to check the preferred alignment of polymeric network. It is observed from the molecular mechanics calculation that existence of additional interaction such as dipole–dipole along with adjustment in other interaction parameter with the change in alignment of polymeric backbone results the increase in the total minimum energy yielding from disturbance in orbital coplanarity with the orientation causing unfeasible state [Ionita and Pruna, 2011; Kumar et al., 2015]. The minimization of energy is calculated for two tentative alignments of ligand in the polymeric chain (Figure 3.7a, b). Herein we have used three

units of DMTD fused together in *syn* (a) and *anti*–alignment (b). The energy minimization calculation validate that the total energy of DMTD–Ag is minimum in case of *anti*–alignment establishing the *anti*–one as favorable due to low bending energy and torsional interaction rather than the *syn* orientation (Table 3.1).

(a) **(b)**

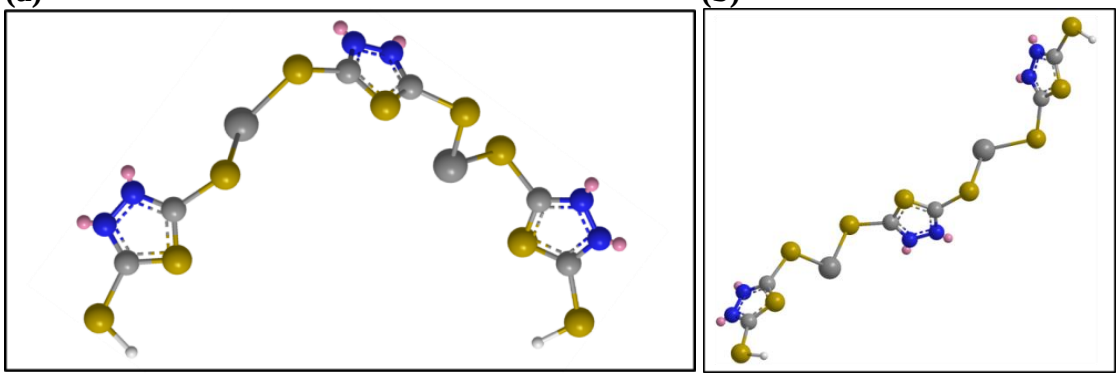

Figure 3.7 Ball–stick model structure of DMTD–Ag in *syn* orientation (a) and *anti*–orientation (b) generated by CS 3D Chembio draw with simple structural energetic minimization. Here blue, white, golden, pale grey, dark grey and pink ball represent N, H, S, C, Ag atoms and lone pairs present in DMTD–Ag.

Table 3.1 Interaction parameters involved in three DMTD–Ag molecular fusions.

Energy (kcal/mol)	***Syn* alignment**	***Anti* alignment**
Stretch	0.4735	0.4276
Bend	14.0841	13.3910
Stretch–Bend	–0.2977	–0.2250
Torsion	1.5293	0.7517
Non 1,4–VDW	–2.6062	–2.0210
1,4–VDW	5.0469	4.2570
Charge–charge	–	–
Charge–dipole	–	–
Dipole–dipole	–5.1269	–5.9172
Total energy	13.1031	10.6641

Where

Bend energy:	araised from displacement of bond angle from their

	equilibrium state
Non VDW:	araised from electrostatic or non atom centered charges.
Stretch energy:	araised from displacement of bond (contraction or elongation) from their equilibrium state
VDW:	van der Waal force: araised from interaction between electron clouds around two non–bonded electrons
Torsion energy:	araised from steric and electrostatic non bonded interaction of atoms
Dipole–dipole:	araised from displacement of electron resulting dipole formation
Charge–charge	araised from displacement of electron resulting dipole formation
Charge–dipole:	araised from interaction of charge and dipole

On the basis of above consequences the structural network of DMTD–Ag is proposed and shown in figure 3.7. It is obvious from the outcomes of FT–IR, Raman spectroscopy and XPS results that Ag(I) get coordinated to DMTD molecule through sulphur atoms in the polymeric chain that is geometrically and symmetrically feasible [Wen et al., 2001]. The linking of sulphur with Ag is in short range order which may be due to twisting of polymeric chain. However there is a possibility of π–π electronic interaction between thiadiazole rings of individual chain that results into small crystallites of low apparent order as evident by XRD experimentation.

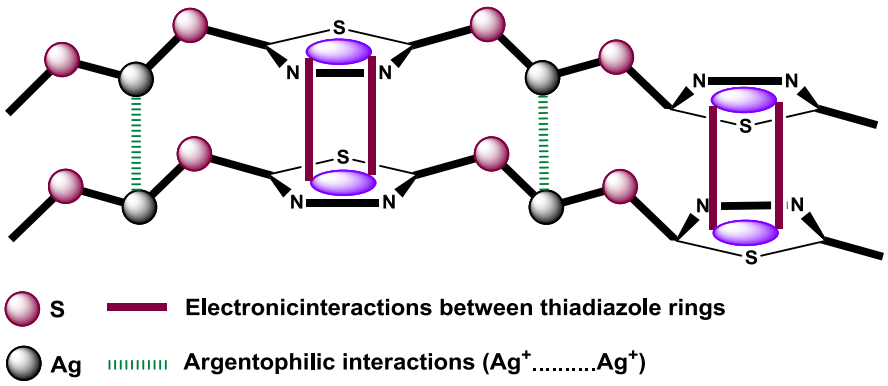

Figure 3.8 Proposed network of DMTD–Ag.

The thermal analysis of DMTD–Ag is investigated using TGA/DTA as shown in figure 3.9. It reveals that the as–synthesized DMTD–Ag is thermally stable up to 200 ºC and its thermal degradation occurs in three steps; corresponding DTA curve exhibit three endothermic peaks at 220 ºC, 380 ºC and 600 ºC. The first decomposition in DMTD–Ag may be due to cleavage of coordination linkage between silver and DMTD. Before that the slight weight loss within temperature range up to 100 ºC reveals the removal of uncoordinated water molecules. Similarly second and third decomposition occurs mainly due to the successive fragmentation of byproducts of DMTD. The activation energy for stepwise decomposition of DMTD–Ag is evaluated by Broido plot [Gupta et al., 2015] as 8.6 kJ/mol, 10.1 kJ/mol and 15.7 kJ/mol for first, second and third stage decompositions respectively. The lowest value of activation energy corresponding to first stage reveals the cleavage of coordination linkage.

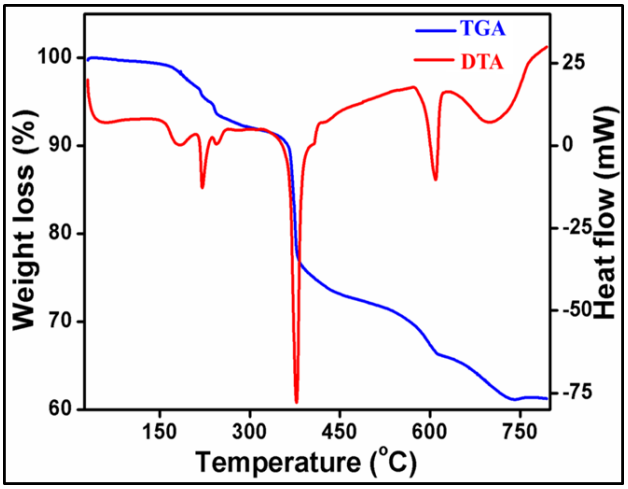

Figure 3.9 TGA and corresponding DTA plot of AMT–Ag.

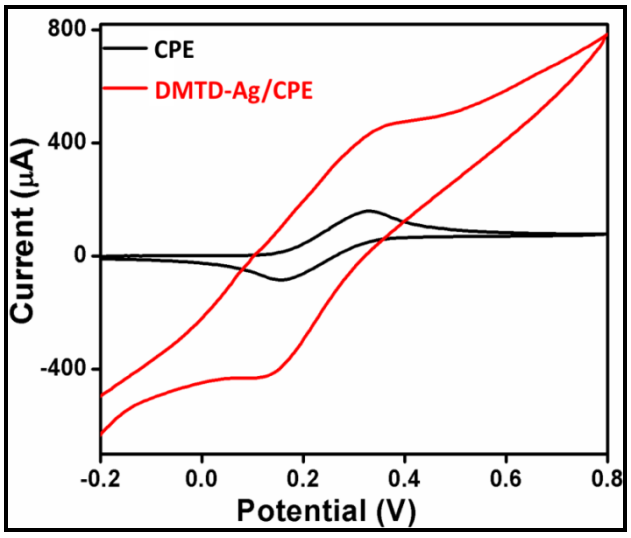

Figure 3.10 CV for 0.01 M Fe(II)/Fe(III) in 0.1 M PBS (pH 10) at unmodified CPE and DMTD–Ag/CPE scans *vs.* Ag/AgCl at 50 mV s^{-1}.

3.3.2 Electro–analytical behavior of DMTD–Ag/CPE

Prior to the voltammetric assay of atropine sulphate, DMTD−Ag/CPE is initially checked for its electron transfer kinetics and then for oxidation behavior of atropine sulphate. The robust electron transfer kinetics of DMTD–Ag/CPE is studied and compared with unmodified CPE by CV technique in presence of 0.01 M Fe(II) /Fe(III) redox couple in 0.1 M phosphate buffer solution (PBS) (pH 10).

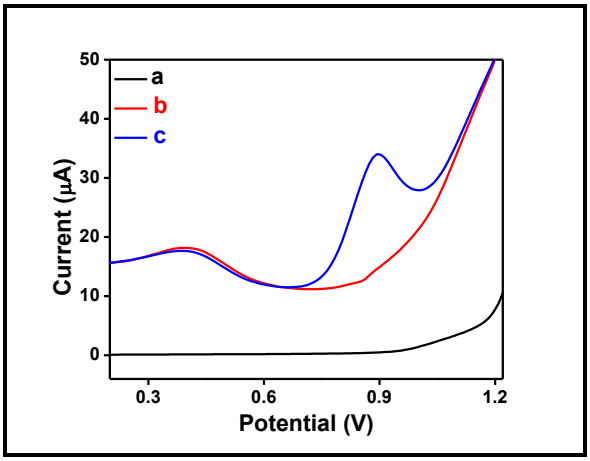

Figure 3.11 DPV of (a) unmodified CPE (b) DMTD–Ag/CPE and (c) DMTD–Ag/CPE + atropine sulphate in PBS pH 10.

Further three electrode arrangements composed of CPE as working electrode, Pt foil as counter electrode and Ag/AgCl as reference electrode is used to check the electroactivity of DMTD–Ag/CPE compared to unmodified CPE at fixed scan rate 50 mV/sec. Compared to the unmodified CPE, DMTD–Ag/CPE shows an increased reversible behavior (Figure 3.10). Hence, it is evident that DMTD–Ag modified CPE can be used as a redox modifier for an analyte. After that the voltammetric behavior of DMTD–Ag/CPE is checked towards oxidation of atropine sulphate in PBS pH 10 (Figure 3.11). The DMTD–Ag/CPE shows increased current with an anodic peak at 0.4 V that is characteristic peak of Ag(I) [Chekin et al., 2014]. However a small amount of atropine sulphate yields an additional anodic peak at 0.9 V which is attributed due to the oxidation of atropine sulphate over DMTD–Ag modified CPE. Thus it is concluded that DMTD–Ag/CPE can be utilized for voltammetric assay of atropine sulphate.

3.3.3 Electrochemical detection of atropine sulphate

After optimization of experimental conditions, trace level of atropine sulphate is electrochemically detected at DMTD–Ag/CPE using DPV. This modified CPE respond quickly to the oxidation of atropine sulphate upon the serial additions of atropine sulphate (Figure 3.12a). The oxidation peak current gradually increases linearly and shifting towards higher potentials with the increase in concentration of atropine sulphate, suggesting diffusion controlled process [Kalanur et al., 2008]. The redox process of DMTD–Ag over CPE and the oxidative mechanism of atropine [Portis et al., 1970; Laube et al., 1977] is depicted in scheme (Figure 3.13). The anodic current increases linearly with the concentration of atropine sulphate in the range from 0.6 μM to 7.0 μM at an R^2 value of 0.98 (Figure 3.12b).

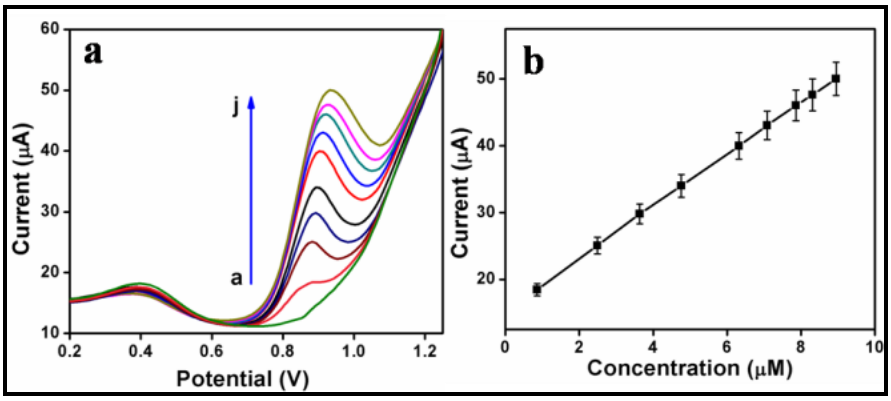

Figure 3.12 (a) DPV response for successive addition of atropine sulphate in PBS pH 10 (a–j) and (b) corresponding calibration plot.

The DMTD–Ag/CPE shows the best linear range compared to earlier reported modified electrode sensors in PBS based supporting electrolyte [Zhou et al., 2011]. The sensitivity was obtained to be 0.02 μA/μM. The limit of detection (LOD) for atropine sulphate assay was calculated to be 46.00 nM with signal to noise ratio (S/N) 3. The excellent sensitivity for eletrodetection of atropine sulphate is caused by uniform dispersion of porous oblong veins of DMTD–Ag at the electrode surface. Consequently, DMTD–Ag supplies a novel potential material for the construction of nonenzymatic electrochemical sensor of high sensitivity over a wide range of concentration and it would be a good supporting matrix.

3.3.4 Analytical performance in clinical formulation

In order to impart further understanding for the potential application of this analytical method towards sensing of atropine sulphate within a ‘true’ sample, that is, one likely to be encountered within daily life applications, a sample of eye drop is utilized. The viability of detection of atropine sulphate is determined within an eye drop buffered to the optimized pH 10. The response of atropine sulphate was explored using

same experimental parameters as employed for drug. Evidently, addition of true sample results in the formation of a clear anodic peak at 0.9 V similar to atropine sulphate.

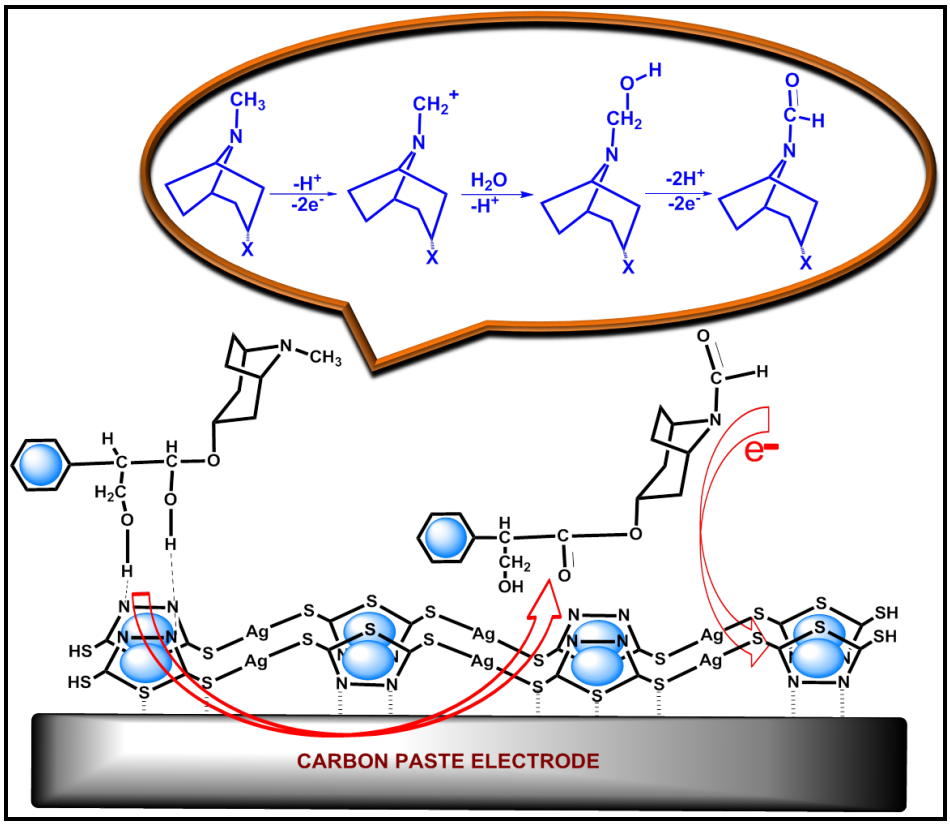

Figure 3.13 A schematic illustration for atropine oxidation at modified electrode. Here X is –OCH(OH)CH(CH_2OH)C_6H_5.

An apparent enhancement in the anodic peak current is scrutinized for the eye drop containing atropine sulphate as described in the voltammogram (Figure 3.14a). A calibration plot of anodic peak current as a function of concentration reveals a linear response over the entire range from 0.6 µM to 7.0 µM with a sensitivity 0.02 µA/µM and limit of detection 72.50 nM as depicted in figure 3.14b.

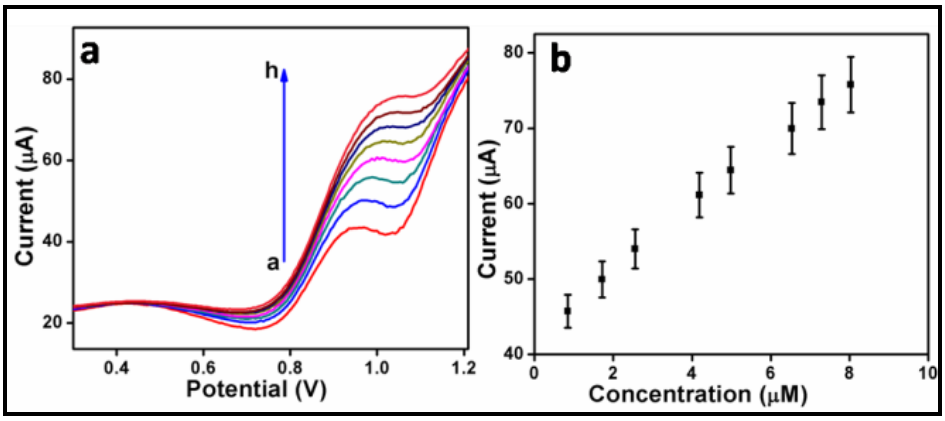

Figure 3.14 (a) DPV response for successive addition of eye drop in PBS pH 10 (a–h) and (b) corresponding calibration plot.

Table 3.2 Analytical figures of proposed work compared with other methods.

Method	**Application**	**Linear range (μmol L^{-1})**	**Detection limit (μmol L^{-1})**	**Regression value**	**Reference**
ISE	Pharmaceutical	17.0–20.0x 10^3	–	0.98	Muldoon et al., 1997
HPLC	Pharmaceutical, biological fluids	2.6–1.3x10^2	2.60	0.99	Papadoyannis et al., 1994
MIP sensor	Serum, urine	8.0–4x10^3	2.00	0.98	Zhu et al., 1993
FIA–ISPs	Pharmaceutical	20.0x10^5	2.00	0.98	Cai, 1993
CV	–	5.0–50.0	3.90	0.98	Ramdani et al., 2013
DPV	Pharmaceutical	0.6–7.0	0.046	0.99	This work

Furthermore, the reproducibility of DMTD–Ag/CPE sensor within the eye drop is highlighted through the inclusion of error bars. A deviation in range and limit of detection of the ideal and true analytical samples are evident, the linear range of calibration plot is analytically useful. The analytical figures of performance for atropine sulphate assay by various reported methods and the proposed method are

tabulated (Table 3.2). The table confirms that limit of detection using the proposed method is the least among the other methods, leading to the epilogue that the proposed strategy manifest a potential role for the atropine sulphate detection.

3.4 Conclusions

Through a systematic analysis of true solution composed of atropine sulphate on DMTD–Ag/CPE, we manifest here a facile and quick approach for development of coordination polymers of DMTD with Ag. As–synthesized DMTD–Ag possesses unique chemical and physical properties due to the tunable, functional pore voids and hetroatoms of DMTD–Ag, it entraps atropine molecules over its surface through hydrogen bonding and responds to the electrode. Moreover, this synthesis method reports a novel smart design of nanostructured porous material capable of sensing the drug–atropine sulphate, overcoming the existing limitations of sensitivity, detection limit etc. The building blocks of ancillary ligand (DMTD) are key components which are readily polymerizable through their thiol groups. The exocyclic sulphur atoms are shackled with Ag(I) leading to the formation of unique porous network of DMTD–Ag. The building blocks are characterized by FT–IR, XPS, Raman spectroscopy and all data are consistent with the as–proposed structural model of DMTD–Ag. Evidently, here the electron transfer is channeled through honeycomb porous veins of DMTD–Ag. In summary, it is shown that redox–active DMTD–Ag can be used to develop a voltammetric sensor based on its brilliant electro activity. The dynamics study of electron transfer for the DMTD–Ag/CPE manifests that it plays the dual role as a redox mediator as well as an electronic conductor. The voltammetric scrutiny further provides anodic peak current linearly dependent with the concentration of atropine sulphate with

sensitivity and limit of detection as 0.02 μA/μM and 46.00 nM respectively. The concentration of clinical formulation, eye drop is also linearly dependent with the anodic peak current with sensitivity 0.02 μA/μM and limit of detection 72.50 nM. These investigations are highly relevant to the frontier of the potential technological applications in sensing area.